Acta Crystallographica Section D
Biological Crystallography
ISSN 0907-4449

High-throughput phase-diagram mapping *via* powder diffraction: a case study of HEWL *versus* pH

Sebastian Basso, Andrew N. Fitch, Gavin C. Fox, Irene Margiolaki* and Jonathan P. Wright*

European Synchrotron Radiation Facility, BP-220, F-38043, Grenoble CEDEX 9, France

Correspondence e-mail: margiolaki@esrf.fr, wright@esrf.fr

Received 5 July 2005
Accepted 6 November 2005

44 samples of tetragonal hen egg-white lysozyme (HEWL) were obtained as a series of polycrystalline precipitates at 277 K and room temperature in the pH range between 6.56 and 3.33. The precipitates were investigated by the collection of high-resolution powder X-ray diffraction data at 295 K, which reveal the tetragonal or orthorhombic forms of lysozyme depending on the temperature and pH of crystallization. The use of a new robotic sample changer greatly facilitated these measurements. LeBail analyses of the powder patterns display a characteristic behaviour for the pH dependence of the tetragonal unit-cell parameters of HEWL crystallized at both temperatures. More detailed analysis shows that molecular replacement can give a suitable starting point for structural refinements, illustrating that powder data can be sufficient for this approach. Pawley or Rietveld refinements that fit a single model to four data sets simultaneously from four samples crystallized at pH values across the range studied benefit from improved powder data quality *via* the anisotropic changes in the unit cell. The Rietveld analysis gave an average structural model with excellent goodness of fit and stereochemistry.

1. Introduction

Powder diffraction has recently been employed to refine small protein structures (Von Dreele, 1999, 2001, 2005; Von Dreele *et al.*, 2000; Margiolaki *et al.*, 2005). The inevitable loss of information arising from the collapse of three-dimensional reciprocal space into a one-dimensional powder diffraction pattern is an obvious disadvantage with respect to single-crystal diffraction. Nevertheless, the powder technique provides complementary information which may be more difficult to obtain *via* single-crystal diffraction. The peak shapes depend on the microstructure of the material and accurate unit-cell parameters can be obtained more easily from high-resolution data (the instrumental resolution is at least an order of magnitude better than that found in a typical single-crystal experiment using an area detector). Moreover, polycrystalline precipitates can be obtained and studied under a wide variety of crystallization conditions which may be inaccessible in slow-soaking or single-crystal-growth experiments. In this paper, we investigate the effect of temperature and pH on the crystallization of hen egg-white lysozyme (HEWL) by high-resolution powder X-ray diffraction, monitoring the evolution of the unit-cell parameters with crystallization conditions. The pronounced anisotropic variation seen for tetragonal lysozyme with changes in the pH of crystal-

lization is exploited in a multi-data-set Rietveld refinement to obtain an average crystal structure over the pH range investigated.

Lysozyme was chosen because it crystallizes rapidly under various conditions and has been extensively characterized (Sauter *et al.*, 2001). We focus on two common temperatures for crystallization experiments, 277 K and room temperature (RT), and the pH range between 6.56 and 3.33. A distinct phase boundary between the two most well studied tetragonal and orthorhombic crystal forms of HEWL was observed between pH 5.3 and 6.14 at RT in agreement with earlier reports (Jollès & Berthou, 1972). However, considerably different behaviour was revealed when crystallization experiments were performed at 277 K: at this temperature the phase transition shifts to higher pH values by 1.0–1.5 units. Although changes in the unit-cell parameters were observed for crystals grown at both temperatures, the tetragonal crystal form of HEWL was more pH-sensitive and exhibited a pronounced and anisotropic variation with changing pH. In contrast, little pH-induced variation in the unit-cell parameters was observed for the orthorhombic form. In this study, we focus primarily on the tetragonal phase crystallized at 277 K.

Anisotropic variations of unit-cell parameters with temperature have recently been suggested as a way of improving powder data quality for structure solution of small-molecular materials (Shankland *et al.*, 1997; Brunelli *et al.*, 2003). When the unit-cell parameters change anisotropically the pattern of peak overlaps is altered, allowing the contributing reflections within a cluster of overlapped peaks to be more easily distinguished. In this paper the same idea is applied to tetragonal lysozyme, where the anisotropic perturbation of the unit cell is caused by the change in the pH of crystallization, leading to an improvement in the data used for structure refinement.

To characterize the crystal structure of the tetragonal phase in these samples, the molecular-replacement method was used to extract initial orientational and positional parameters for the molecule in the unit cell, starting from a previously reported structural model. Multi-pattern stereochemically restrained refinements, originally designed for the extraction of average structural models, were employed for deriving and refining the structure in the 6.56–3.33 pH range at 277 K. Our refined model for the tetragonal structure gives a good fit to the powder data throughout the pH range, with the changes as a function of pH being modelled by differences in the bulk solvent. This multipattern methodology offers great potential for structure analysis of systems with large unit cells using powder diffraction data owing to the improvement in data quality.

2. Experimental

2.1. Crystallization

Hen egg-white lysozyme (HEWL) was purchased from Sigma–Aldrich chemical company (product No. L7651, Lot 091K7021; CAS No. 12650-88-3). The crystallization method used was the salting-out procedure in batch mode. The stock protein solution was prepared by adding 3011 mg of as-received dry lysozyme to 30 ml of 0.1 *M* buffer solution. The initial pH value of the ammonium acetate buffer solution was measured using a pH meter (GLP 21, Crison) to be 7.17. 1 *M* sodium hydroxide solution was then added to increase the pH value of the starting solution to 8.00 and this stock solution was then decreased to pH 3.35 in a systematic manner in steps of roughly 0.2 pH units initially using 1 *M* hydrochloric acid and then 5 *M* hydrochloric acid starting at pH 5.45. In each step, 500 µl of the buffered protein solution was extracted and placed in one well of each of two 24-well batch crystallization plates (Hampton Research). An equal volume (500 µl) of 1.2 *M* sodium chloride solution was added (either at RT or in a cold room at 277 K) to each well of the plates, giving a final protein concentration of 50 mg ml^{-1} and a salt concentration of 0.6 *M*. At low temperatures the mixing resulted in immediate precipitation. Over the next few days polycrystalline precipitates were visible at the bottom of the wells of each tray, with clear solution above. All samples were loaded into 1 mm diameter glass capillaries and centrifuged for approximately 15 min in order to enhance the packing of the protein crystals. Excess mother liquor was removed and the capillaries were sealed with wax to prevent protein dehydration. All samples were ∼10 mm long.

Owing to the relative acidity of the lysosyme molecule (estimated pK_a = 11), the pH of the solution is expected to change as the protein crystallizes out, giving a final value [$pH_{(f)}$] which is different to the initial value [$pH_{(i)}$]. This problem is most apparent at high pH values which are outside of the optimal buffering range of ammonium acetate. Therefore, the pH values of the solutions from both crystallization plates were measured again just before the diffraction experiment to give the final values (see supplementary material[1]). In the course of this work, we report only 20 samples prepared at RT since contamination and/or slight increases of pH with respect to the expected values after crystallization were observed for the other four specimens. Hereafter, each sample (from the 277 K experiment) will be referred to as pH*X*, where *X* corresponds to the measured $pH_{(f)}$ of the protein solution.

2.2. X-ray data collection and processing

Powder X-ray diffraction data for all 44 samples were collected at room temperature using synchrotron radiation at the high-resolution powder diffraction beamline ID31, ESRF, Grenoble (Fitch, 2004). The nine analyser crystals which are separated by ∼2° were scanned over a 20° range in 2 min with a sampling time of 3 ms. Eight scans per sample were collected, with the capillary being translated on every other scan to expose a fresh region of sample unaffected by radiation damage. Owing to the rapid data collection, high-speed

[1] Supplementary material has been deposited in the IUCr electronic archive (Reference: SX5038). Details for accessing these data are described at the back of the journal.

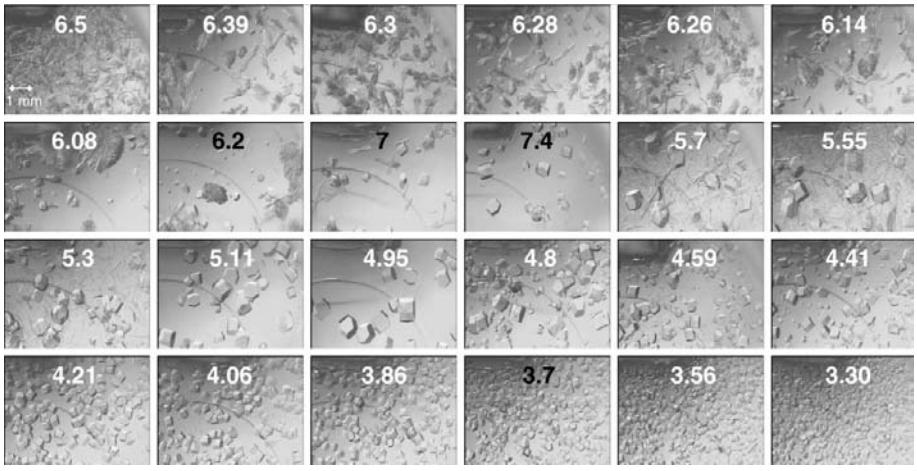

Figure 1
Pictures taken on an optical microscope of the HEWL crystals from all 24 wells of the pH-variation experiment at RT, from pH 6.5 to 3.30, where each number represents the $pH_{(f)}$ of the medium. In our study only 20 samples are reported since contamination after crystallization was observed for the four specimens in black.

spinning (3000 rev min^{-1}) of the samples is necessary in order to ensure adequate powder averaging. Hence, samples were mounted on a fast capillary spinner which also allows the sample to be translated along the axis of the diffractometer. An automatic sample-changing robot (Stäubli-Automazioni), recently installed at ID31, was used for loading and unloading all the samples by mounting the capillaries in auto-centring magnetic bases. Data collection on 24 capillaries resulting from one of the plates was completed overnight, with the second tray being measured during the next night. The chosen wavelength of 1.249826 (9) Å gives particularly high resolution, in terms of minimum instrumental contribution to the widths of the diffraction lines, and low-angle asymmetry effects were reduced by using an appropriate incident beam size (1.5 mm horizontally by 1.0 mm vertically). Radiation-damage effects are accompanied by considerable changes in unit-cell parameters along with gradual increases in peak broadening and can be monitored by comparing the profile measured in each of the nine channels during a single scan, as well as by comparing subsequent scans. The first scans, where the sample had been translated to give fresh material, were combined, leading to increased counting statistics without compromising the data quality for structure analysis, while the second scans showed detectable degradation and were not used in the subsequent analysis.

3. Variation of HEWL with pH

3.1. Indexing of powder profiles and space-group assignment

Data analysis was carried out in a systematic way using positions extracted from the first 20 lines of the high-resolution powder diffraction profiles collected for all 44 samples crystallized at different pH values. For example, a tetragonal unit cell was found for sample pH6.36 with unit-cell parameters a = 78.8437, c = 38.188 Å and figures of merit $M(20)$ = 60.2 and $F(20)$ = 821.9 by employing the *DICVOL* program (Boultif & Louër, 1991). This unit cell is in agreement with the expected tetragonal phase for HEWL crystallized under these conditions. A probabilistic approach for the space-group determination (Markvardsen *et al.*, 2001) incorporated into the *DASH* software package (David *et al.*, 1998) indicated that the extinction symbol $P4_12_1-$ accounts for the systematic absences for the pure phase, giving as possible

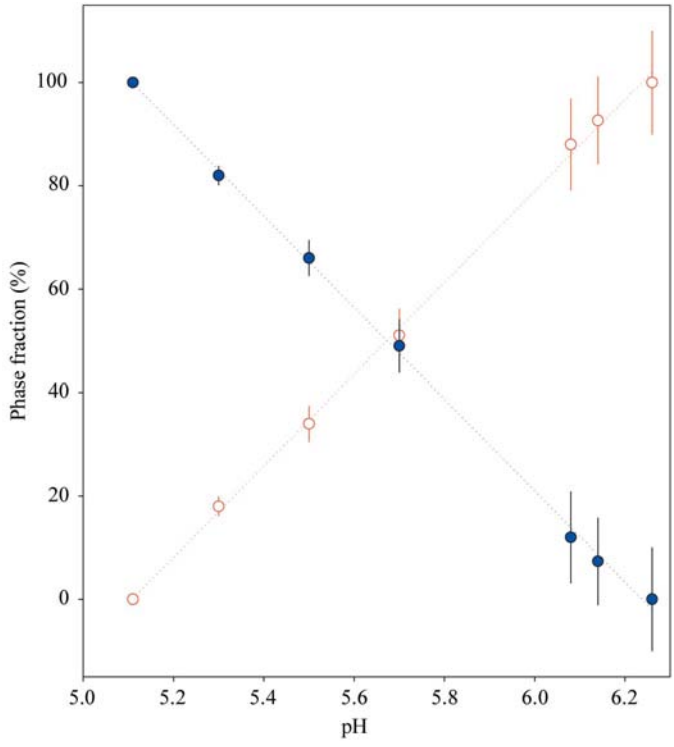

Figure 2
Evolution of the fractions (%) of the tetragonal and orthorhombic phases observed in HEWL in the pH range 5.11–6.26. The solid blue symbols correspond to the tetragonal phase and the open red symbols correspond to the orthorhombic phase. The errors are equal to 10% of the observed values. The dotted lines are guides for the eye.

space groups $P4_12_12$ or $P4_32_12$. Previously reported results for HEWL indicate that $P4_32_12$ is correct and therefore the analysis was performed using this space group, in which there is one molecule in the asymmetric unit and a Matthews coefficient of 2.12 Å^3 Da^{-1} for crystals with 41.39% solvent content in the unit cell. The same space group ($P4_32_12$) was found to be suitable for all the tetragonal phases prepared at different pH values.

The indexing figures of merit were similar for all the other tetragonal samples with the exception of samples pH6.56, pH6.51 and pH6.41 and samples crystallized from pH 6.14 to pH 5.30 at RT, which showed extra diffraction lines that could be accounted for by the $P2_12_12_1$ orthorhombic phase of HEWL (Biswal *et al.*, 2000). At 277 K the tetragonal phase dominates the phase diagram, in agreement with previous studies (Judge *et al.*, 1999), while traces of the orthorhombic phase were only observed in the three highest pH samples. On the other hand, at room temperature phase-pure tetragonal samples were obtained at low pH only, with a co-existence region between pH 6.14 and pH 5.30 and a pure orthorhombic phase above pH 6.14. This was observed by simple visual observation of each well of the tray using an optical microscope in the early stages (Fig. 1). The fractions (%) of the two phases in the co-existence region at RT have been calculated as percentages of the total integrated intensities using the LeBail method with the *FULLPROF* suite of programs (Rodriguez-Carvajal, 1993) and can be seen in Fig. 2. The 'tipping point' in terms of the percentage occurrence of each form at RT lies in a narrow range between pH 5.5 and pH 5.8.

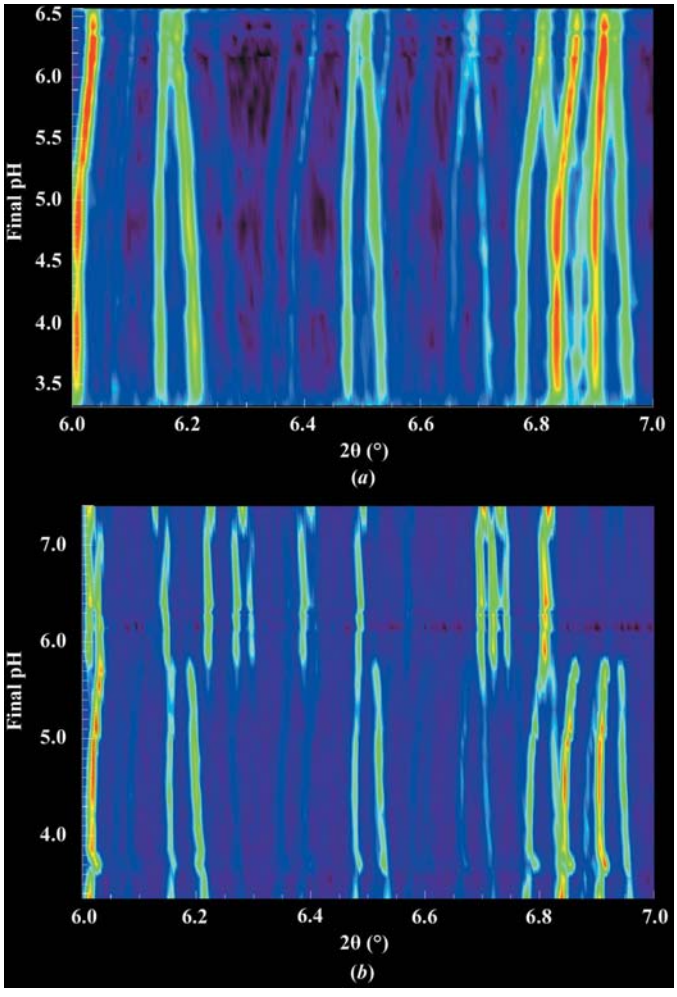

Figure 3
Colour representation of ID31 powder diffraction data from the pH-variation experiment from pH 6.56 to 3.33 of HEWL crystallized at 277 K (*a*) and RT (*b*). At low temperature, the tetragonal phase is favoured as a smooth anisotropic shift in the peak position is apparent.

3.2. LeBail analysis for the extraction of accurate lattice parameters

Further data analysis was performed with the *General Structural Analysis Software* (*GSAS*; Larson & Von Dreele, 2004) using the *EXPGUI* graphical user interface (Toby, 2001). In order to obtain reliable values of the unit-cell parameters and characterize the peak shape and background coefficients without a structural model, a LeBail fit (LeBail *et al.*, 1988) was initiated with a phase-pure tetragonal sample pH6.36. In the course of the refinement, the shape of the diffraction lines could be well described by the profile function of Finger *et al.* (1994), which models peak asymmetry arising from axial divergence. Parameter values were refined during

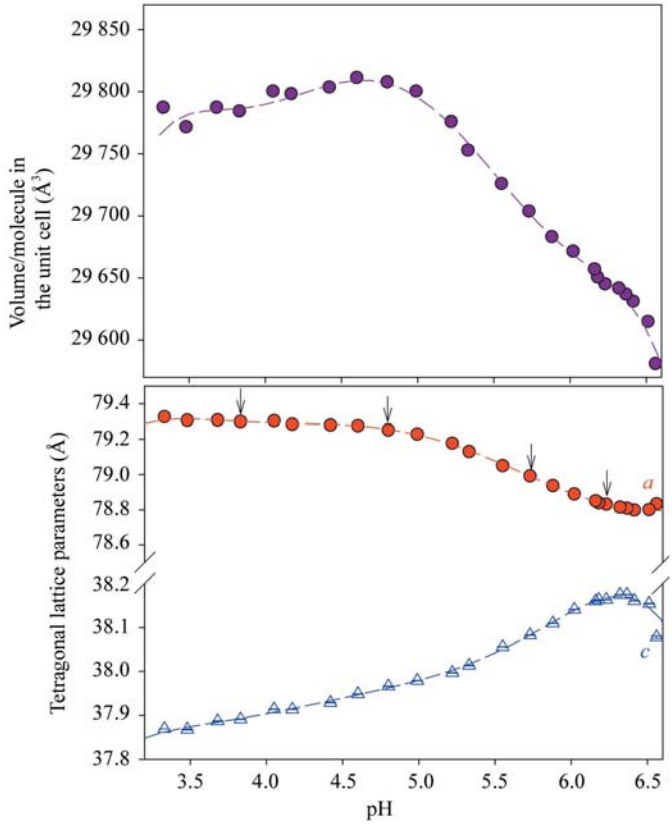

Figure 4
Variation of unit-cell dimensions (lower) and volume (upper) from ID31 data for tetragonal HEWL with the pH of protein solution after crystallization is complete at 277 K. Note that the error bars are much smaller than the observed variations. The dashed lines are guides for the eye. The arrows indicate the four data sets employed for Rietveld analysis (§3.5).

the early stages of analysis and were subsequently fixed to $S/L = 0.12 \times 10^{-2}$ and $H/L = 0.64 \times 10^{-2}$. Further improvements in the fit were achieved when anisotropic size and strain broadening of the peaks were allowed to refine. The pattern-decomposition procedure converged with $R_{wp} = 4.81\%$ and tetragonal unit-cell parameters $a = 78.8089\,(5)$, $c = 38.1747\,(6)$ Å.

At 277 K, a smooth variation of the tetragonal unit-cell parameters and volume per molecule with pH (see supplementary material) was observed when this analysis was repeated systematically for all other diffraction profiles. Direct visualization of the collected profiles in a comparative way indicates a clear anisotropic shift of the peak positions with pH (Fig. 3*a*). This observation arises from an anisotropic variation of unit-cell parameters with pH and is quantified by these LeBail fits. Fig. 4 shows that the crystallographic axis *a* decreases by $\delta a/a_0 = 0.61\%$ and *c* increases by $\delta c/c_0 = 0.55\%$ with increasing pH from 3.33 to 6.56 at 277 K. Similarly, the decrease in the volume per molecule of the tetragonal unit cell ($Z = 8$) is $\delta V/V_0 = 0.67\%$.

The refined error bars give the precision of the unit-cell parameters as $\delta a/a = 5 \times 10^{-6}$ and $\delta c/c = 1 \times 10^{-5}$. Taking into account the systematic errors arising from the wavelength calibration, modelling of the axial divergence and heat-load changes in the optics, the absolute accuracy is estimated to be at least one part in 10^4. The changes in unit-cell parameters with pH are more than 50 times greater than this conservative estimate, indicating that these quantities are well determined experimentally. The use of a high-resolution parallel-beam geometry (equipped with analyser crystals) means that the data are free from many geometric aberrations. Compared with the unit-cell parameters derived from typical area-detector single-crystal experiments, these data are not affected by sample–detector distance and non-perfect crystal centring, as well as being about an order of magnitude sharper in angular resolution. Accurate unit-cell parameters are particularly important for crystal structure refinement when geometric restraints need to be computed using the unit-cell parameters.

A similar LeBail analysis was performed on the samples from the RT experiment, which produced results given in the supplementary material. Plots of these results (Fig. 5) demonstrate that the behaviour of the tetragonal phase seen at 277 K is an intrinsic property of HEWL as the same variation of the unit-cell parameters takes place. Fig. 5 depicts the results for the orthorhombic phase, from which it is clear that this phase is much less sensitive to pH effects over the

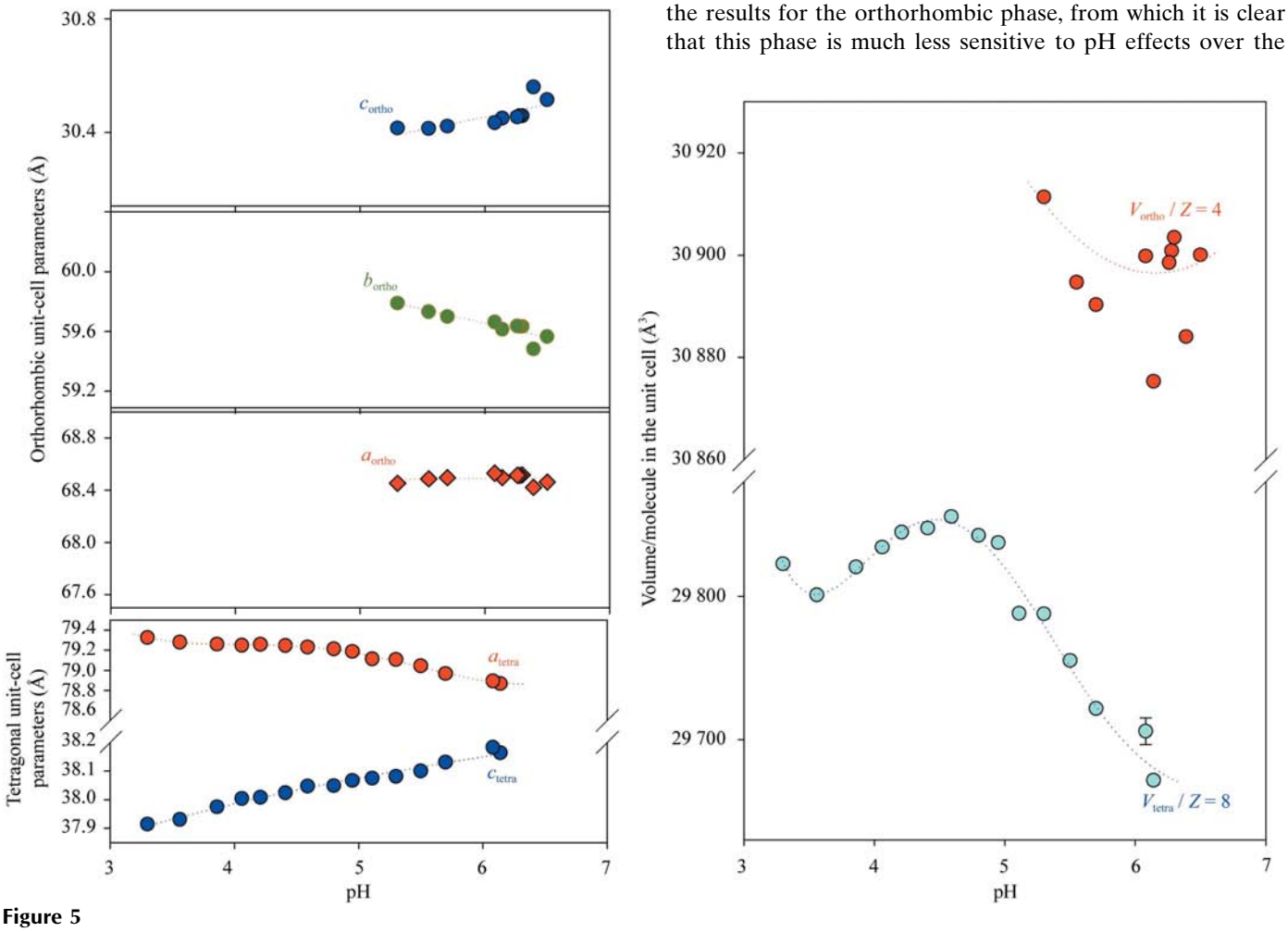

Figure 5
Variation of unit-cell parameters (left) and volume (right) from ID31 data for tetragonal (bottom) and orthorhombic (top) HEWL with the pH of protein solution after crystallization is complete at RT. Note that the error bars are much smaller than the observed variations. The dashed lines are guides for the eye.

range examined. A comparative visualization of the collected profiles for the samples crystallized at RT (Fig. 3*b*) verifies this observation. In the following sections, we aim to derive insights into the variations of the tetragonal phase with pH at 277 K in an attempt to gain a better understanding of the observed unit-cell alterations.

3.3. Molecular replacement and rigid-body minimization: orientation and position of the protein molecule in the unit cell

Our earlier work on turkey egg-white lysozyme (TEWL) using powder diffraction data showed that use of the molecular-replacement method can result in the extraction of reliable values for the three positional and three orientational parameters required for the description of a molecule in the unit cell (Margiolaki *et al.*, 2005). In this case, integrated intensities were extracted from the LeBail fits described in §3.2 where the best profiles, which are representative of the higher and lower regions of pH under study, were chosen (samples pH6.23 and pH3.83). In total, 2050 intensities were extracted up to a maximum resolution of 3.27 Å from the data collected for sample pH6.23 (R_{wp} = 4.19%, χ^2 = 1.47). These extracted intensities were then imported into the *CCP*4 software suite (Collaborative Computational Project, Number 4, 1994; Potterton *et al.*, 2003) to provide input into the molecular-replacement program *MOLREP* (Vagin & Teplyakov, 1997). PDB entry 193l (Vaney *et al.*, 1996) refined at 1.33 Å resolution for tetragonal HEWL was employed as a starting model, taking into account only the protein atoms. The good quality of these data allowed the extraction of a reliable solution for both the rotation (first solution, R_f/σ = 4.2; second solution, R_f/σ = 3.38) and translation functions (first solution, correlation coefficient = 0.51; second solution, correlation coefficient = 0.37), clearly distinguished from the rest of the peaks (Fig. 6). The same procedure was followed using the extracted intensities from the profile collected for the sample pH3.83, resulting in a second position and orientation. After careful examination of the two solutions, it was clear that they are both related by symmetry to the original model by the affine normaliser ($\frac{1}{2}$, $\frac{1}{2}$, 0) of the tetragonal space group ($P4_32_12$),

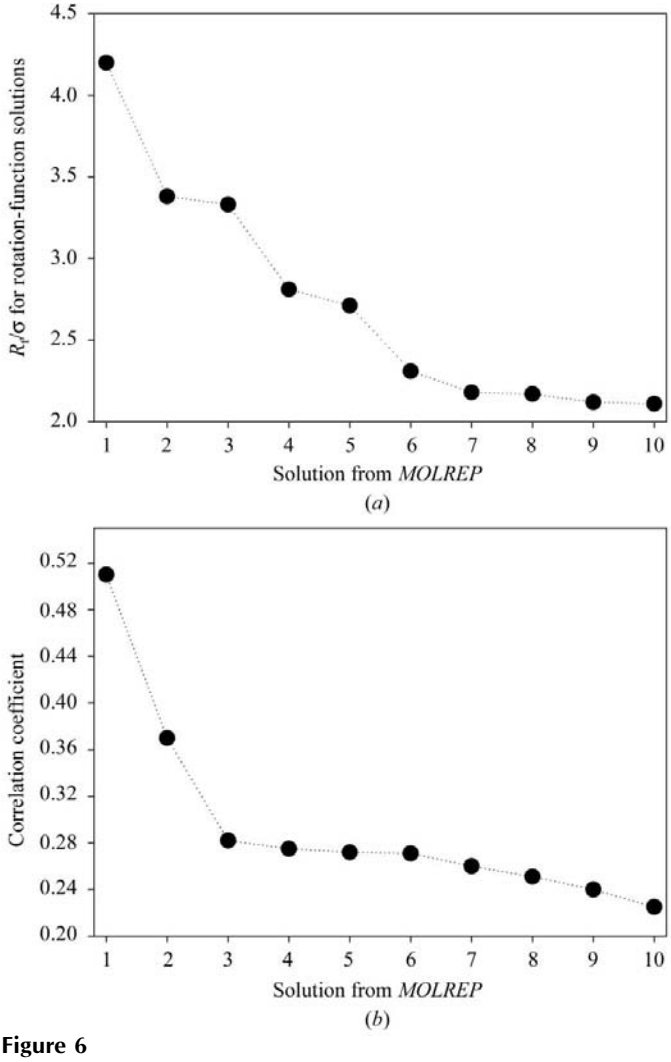

Figure 6
(*a*) *R* factor/σ computed for rotation-function solutions and (*b*) correlation coefficients computed for molecular replacement using model 193l (tetragonal HEWL) and intensities extracted from the LeBail refinement for sample pH6.23 (see text). The top ten rotation-function peaks were each used to generate ten translation-function peaks using the *MOLREP* program.

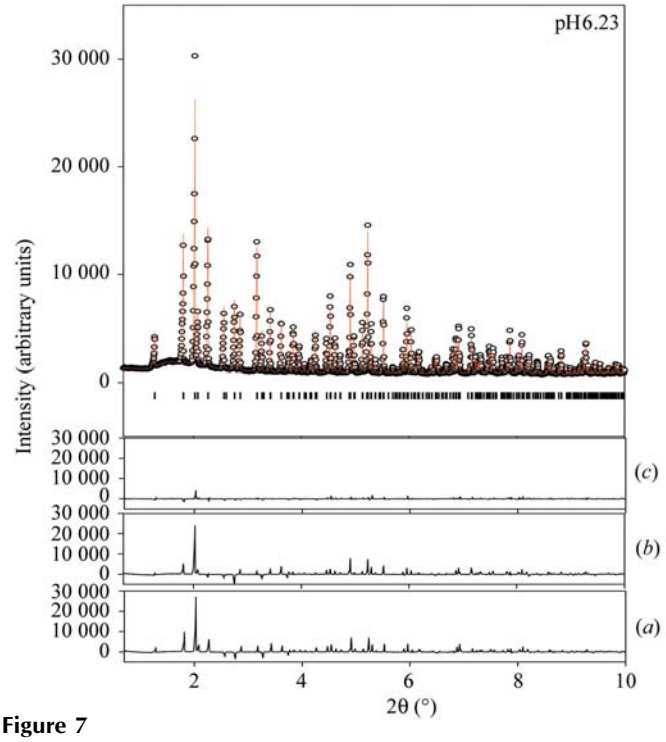

Figure 7
Selected part of the Rietveld fit for sample pH6.23 (upper panel) and the evolution of the agreement between the observed and calculated profiles after performing (*a*) molecular replacement [R_{wp} = 22.60%, $R(F^2)$ = 46.87%], (*b*) rigid-body refinement [R_{wp} = 19.47%, $R(F^2)$ = 21.39%] and (*c*) final restrained refinement of the atomic coordinates [R_{wp} = 7.35%, $R(F^2)$ = 13.65%]. The data were collected at 295 K [ID31, λ = 1.249826 (9) Å]. The open symbols, red and lower black lines represent the experimental data, calculated patterns and the difference between experimental and calculated profiles, respectively. The vertical bars correspond to Bragg reflections compatible with the refined tetragonal structural model. The background intensity has been subtracted for clarity.

verifying the robustness of the method and the validity of the obtained solution in this case.

In order to confirm the agreement between measured and calculated patterns based on the best solution obtained from *MOLREP*, a Rietveld refinement (Rietveld, 1969) was initiated in *GSAS*. At this point, only the background, peak shape, unit-cell parameters, scale factor and solvent-scattering coefficients were allowed to vary. The initial agreement factors calculated using data between 102 and 3.27 Å resolution were R_{wp} = 22.60% and $R(F^2)$ = 46.87%. The starting model was subjected to several cycles of rigid-body refinement that improved the fit to give R_{wp} = 19.47% and $R(F^2)$ = 21.39% for sample pH6.23 (Fig. 7). During the rigid-body refinement the molecule rotated by about 5° and translated by approximately 0.5 Å. Although the initial profile *R* factors were high, the packing of the protein molecules in the crystal was assumed to be correct as indicated by the molecular-replacement results.

3.4. Multi-data-set Pawley refinements and data evaluation

In order to identify any differences in peak intensities among the 24 profiles collected from samples throughout the pH range between 6.56 and 3.33 at 277 K, a multi-data-set Pawley refinement (Pawley, 1981) was performed using the *PRODD* profile-refinement program (Wright & Forsyth, 2000; Wright, 2004). The patterns were fitted using the same integrated intensities to model each pattern, but different unit-cell parameters. Any differences in the diffracted intensities would then be highlighted *via* mismatches in the constrained fit. Four patterns corresponding to samples pH3.83, pH4.80, pH5.73 and pH6.23 (T = 277 K) were selected for this purpose.

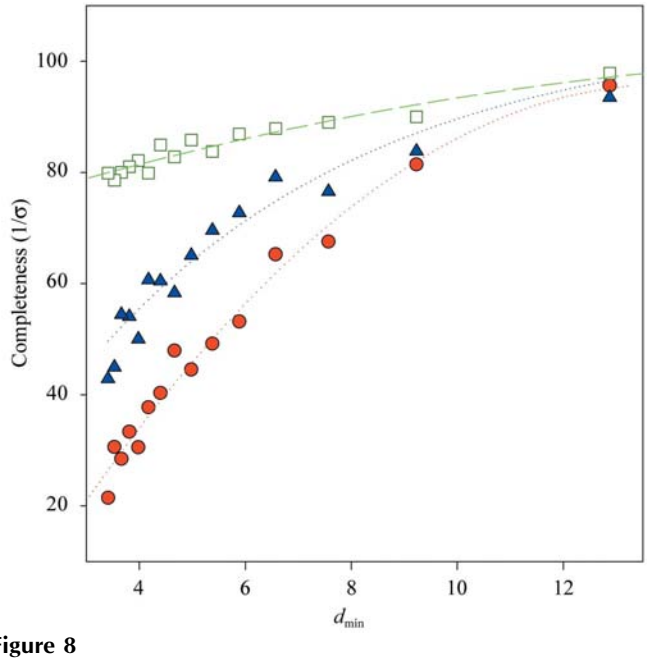

Figure 8
Effective completeness for the powder diffraction data at the 1σ level (see text). Red circles represent a single powder pattern, blue triangles a combined fit to four patterns and the open squares show the maximum completeness attainable in this case, owing to symmetry-overlapped peaks. The dotted lines are guides for the eye.

Table 1
Rietveld refinement results using four high-resolution profiles collected for samples pH6.23, pH5.73, pH4.80 and pH3.83 with a wavelength of 1.249826 (9) Å [2θ range 0.7–22°; resolution range, 102–3.27 Å; $\Delta 2\theta$ = −0.00215 (4)°].

Rietveld refinement	pH6.23	pH5.73	pH4.80	pH3.83
N_{ref}	2124	2077	2046	1929
$N_{restraints}$	5408	5408	5408	5408
N_{steps}	5316	5315	5312	5116
$N_{obs} = N_{restraints} + N_{steps}$	10724	10723	10720	10524
$N_{parameters}$	3015	3015	3015	3015
R_{wp} (%)	7.35	9.85	9.91	9.3
R_{exp}† (%)	2.73	3.76	3.55	4.11
R_p (%)	5.11	6.76	6.56	6.74
R_F^2 (%)	13.66	15.55	15.2	20.23
Total *R* factors for the four histograms: R_{wp} = 8.86%, R_p = 6.08%				
Profile parameters (No. 5) (Larson & Von Dreele, 2004)				
Y	11.1 (2)	9.6 (2)	11.8 (2)	11.3(1)
Y_e	6.8 (4)	7.2 (4)	7.9 (4)	6.8 (6)
D11	0	0.0093 (1)	0.0326 (1)	0.0221 (2)
D33	0	0.006 (1)	0.056 (1)	−0.009 (2)
PROCHECK results				
Bond error (Å)	0.13			
Angle error (°)	2.4			
Residues in core region (%)	83.2			
ω torsion-angle error (°)	1.1			
Bad contacts per 100 residues	2.6			
ζ-angle error (°)	0.3			
Hydrogen-bond energy error (kJ mol^{-1})	2.2			

† $R_{exp} = 1/(\sum w_i y_i^2)^{1/2}$.

Reflections with a reasonable signal-to-noise ratio could be observed in all data sets up to a maximum resolution of 3.27 Å. The combined fit gives slightly poorer agreement indices (*e.g.* pH6.36: R_{wp} = 4.51 *versus* R_{wp} = 3.73) compared with individual fits for each pattern as the peak intensities are constrained to be equal in all four patterns and the tendency to fit the noise in the data with the multitude of overlapping peaks is reduced. The main difference between profiles is the anisotropic variation of the unit-cell parameters with pH discussed in §3.2, with relatively small differences in peak intensity being evident in the difference curves for the low-angle peaks. The differences between the intensities in the different profiles is judged to be insignificant compared with the difference between the starting model and any of the profiles (R_{wp} = 19.47% for the model from molecular replacement is four times worse than that with the intensities constrained to be equal). No sudden changes in any of the peak intensities as a function of pH could be detected from these data.

The least-squares matrix from this Pawley refinement gives information about the data quality. Sivia (2000) has described how the eigenvalue spectrum of the matrix is related to the effective error bar on the extracted intensities (or linear combinations of intensities when peaks are overlapped). In order to give an easier comparison with single-crystal data-processing statistics we have computed the eigenvalues and eigenvectors of a matrix which has rows and columns multiplied by the intensities themselves. In the case of non-overlapping peaks, *e.g.* single-crystal data, this matrix has

$[I/\sigma(I)]^2$ directly as the diagonal matrix elements with off-diagonal elements being zero and the eigenvalue–eigenvector transformation is not needed. When there are significant peak overlaps we choose linear combinations of intensities which are uncorrelated *via* the eigenvalue–eigenvector transformation. We propose that the eigenvalues are closely related to $[I/\sigma(I)]^2$ for the linear combinations of peaks which have been resolved in the powder experiment. In a conventional eigenvalue–eigenvector decomposition the eigenvectors have unit 2-norm ($\sum |v_i|^2 = 1$) and we suggest that the eigenvalue represents $[I/\sigma(I)]^2$ for the linear combination of peaks corresponding to that eigenvector. In order to generate statistics which are independent of the choice of intensity partitioning, we normalize the eigenvectors to have unit 1-norm ($\sum |v_i| = 1$). A detailed justification for these computations will be given elsewhere (Wright, 2005). The *d*-spacing for a linear combination of peaks is then computed as the weighted average of the *d*-spacings of the contributing peaks. An effective completeness for combined data set is proposed as the fraction of 'peaks' having $I/\sigma(I)$ greater than some threshold (3 and 1 were chosen here) and this is tabulated in the supplementary material and plotted in Fig. 8. These numbers are also compared with the number of peaks that could be resolved given the tetragonal symmetry [peaks with Miller indices (h, k, l) and (h', k', l') where $h^2 + k^2 + l^2 = h'^2 + k'^2 + l'^2$ give identical *d*-spacings for tetragonal unit cells].

3.5. Structure refinement *via* the Rietveld method

Owing to the absence of any clear indications of structural modifications *versus* pH, a four-histogram stereochemically restrained Rietveld refinement (Rietveld, 1969) was carried out in order to extract an average structural model for the tetragonal phase of HEWL using the *GSAS* software. The restrained least-squares procedure has been described in detail elsewhere (Von Dreele, 2005) and has been previously applied to metmyoglobin (Von Dreele, 1999), human insulin (Von Dreele *et al.*, 2000), sugar binding to HEWL (Von Dreele, 2001, 2005) and TEWL (Margiolaki *et al.*, 2005). In the present case, the same profiles used for the Pawley refinement were selected in order to proceed with the final structure refinement.

The anisotropic changes in the unit cell were taken into account by using a special profile function implemented in *GSAS* (No. 5; Larson & Von Dreele, 2004). In this function only one set of unit-cell parameters is refined and those corresponding to the rest of the profiles are related *via* a strain $(\delta d/d)$ of the reciprocal metric tensor elements and parameters

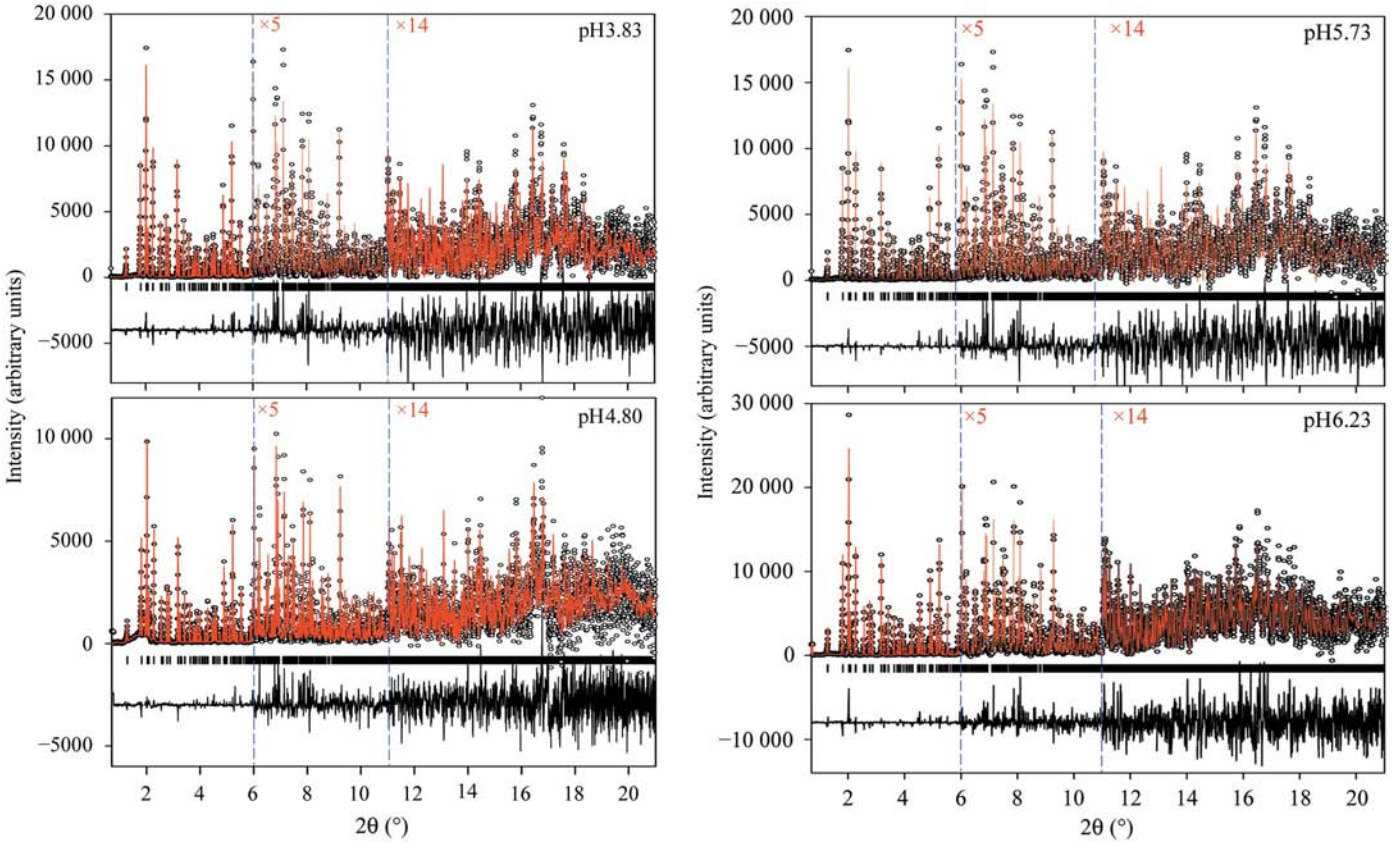

Figure 9
The multi-data-set Rietveld refinement for samples pH6.23, pH5.73, pH4.80 and pH3.83 crystallized at 277 K. The data were collected at 295 K [ID31, λ = 1.249826 (9) Å]. The open symbols, red and lower black lines represent the experimental data, calculated patterns and the difference between experimental and calculated profiles, respectively. The vertical bars correspond to Bragg reflections compatible with the refined tetragonal structural model. The profiles have been expanded by a factor of 5 for Bragg angles in the 6–11° region and a factor of 14 in the 11–21° 2θ region. The background intensity has been subtracted for clarity.

related to the strain are refined in the least-squares procedure. An isotropic temperature factor $U_{iso} = B_{iso}/8\pi^2 = 0.30$ Å^2 was initially used for the description of the thermal motion of all atoms and it was allowed to refine only at the latest stages of the refinement to a value of 0.454 (2) Å^2. A band-matrix approximation implemented in the *GSAS* software was employed with a matrix bandwidth of 20 parameters. In total, 5408 stereochemical restraints were imposed in order to refine the positions of 1001 protein atoms in the asymmetric unit using experimental data between 102 and 3.27 Å resolution. The refinement proceeded smoothly for all four profiles, leading to good quality of the fit (total agreement factors: R_{wp} = 8.86%, R_p = 6.08%). Periodical evaluations of the protein stereochemistry were essential to monitor the progress of the refinement. The evaluation software *PROCHECK* (Laskowski *et al.*, 1993) and *WHATCHECK* (Hooft *et al.*, 1996) and energy minimizations using the *Swiss-PdbViewer* package (Guex & Peitsch, 1999) and *WebLab Viewer Pro* 3.2 (Molecular Simulations Inc.) were all employed to improve the model during the course of the structure refinement.

Details of this refinement are listed in Table 1 and the resulting fitted powder diffraction profiles are presented in

Table 2
Correlation coefficients of intensity differences at the end of the four-pattern Rietveld refinement.

	ΔI_1	ΔI_2	ΔI_3	ΔI_4
ΔI_1	1			
ΔI_2	0.722345	1		
ΔI_3	0.384042	0.519906	1	
ΔI_4	0.326747	0.371463	0.660829	1

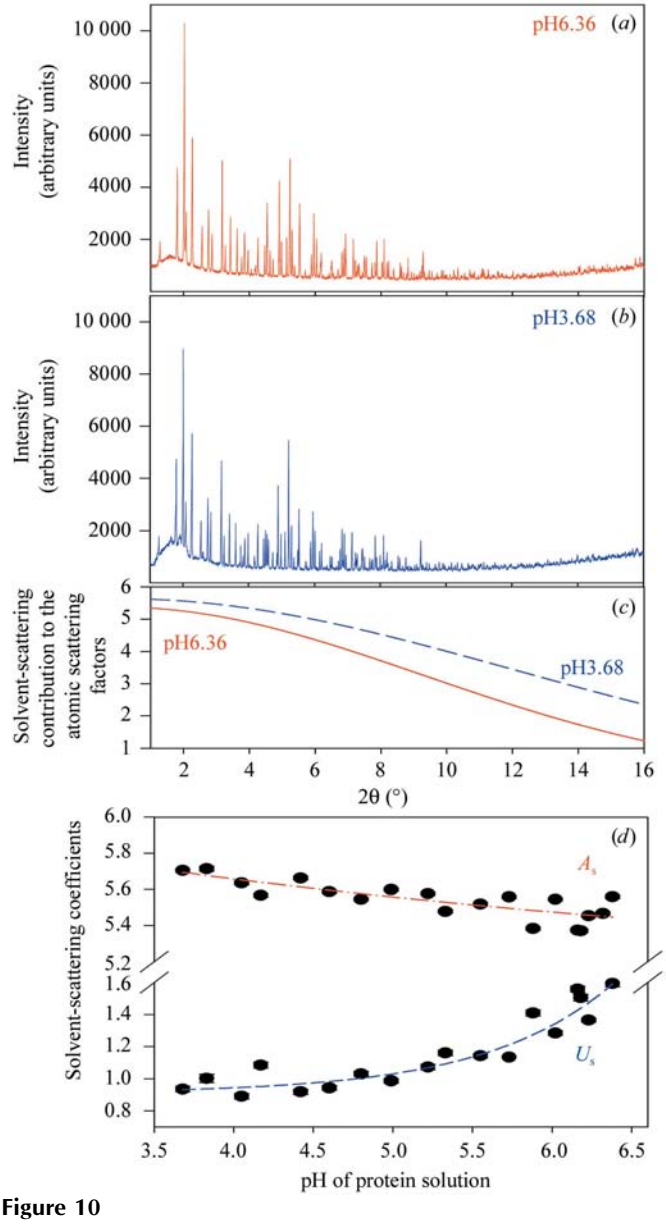

Figure 10
X-ray powder diffraction profiles for (*a*) sample pH6.36 and (*b*) sample pH3.68. (*c*) Solvent-scattering contribution to atomic scattering factors according to Babinet's principle (Larson & Von Dreele, 2004) calculated for samples pH6.36 (red solid line) and pH3.68 (blue dashed line). (*d*) Variation of solvent-scattering refined coefficients with pH (A_s, U_s; see text).

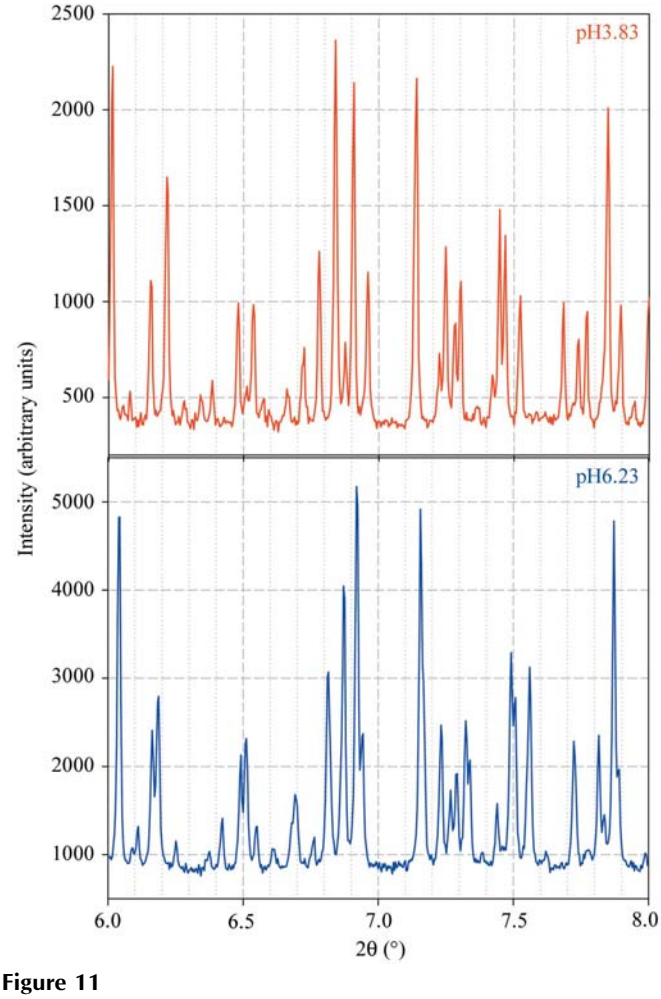

Figure 11
Magnification of the 6–8° 2θ regime of the high-resolution powder diffraction profiles collected for tetragonal HEWL samples (space group $P4_32_12$) pH6.23 [bottom; a = 78.8242 (3), c = 38.15831 (9) Å, V = 237087 (2) Å^3] and pH3.83 [top; a = 79.2996 (6), c = 37.8911 (5) Å, V = 238275 (3) Å^3]. The data were collected at 295 K [ID31, λ = 1.249826 (9) Å].

Table 3
R.m.s. deviations (Å) between the current refined model and previously reported models for HEWL derived from *Swiss PDB Viewer* (Guex & Peitsch, 1999).

Model	Current refined average model	193l	1ja2	1ja6
Current refined average model	—	1.05	0.84	0.79
193l	1.05	—	1.32	1.08
1ja2	0.84	1.32	—	0.86
1ja6	0.79	1.08	0.86	—

Fig. 9. Two coefficients (A_s and B_s) were refined to account for the solvent scattering (Larson & Von Dreele, 2004) *via* a Babinet's principle model. These coefficients were varied separately for each of the different patterns corresponding to different pH values and they can therefore account for some of the small differences in peak intensities at low angle between the different profiles. Additional Rietveld refinements of the individual profiles at all pH values were performed using the refined model (with fixed coordinates) from the multi-data-set Rietveld procedure described above. In this way, the evolution of the A and U coefficients with pH was obtained (Fig. 10). Fig. 11 illustrates a small region of the profiles collected for samples pH6.23 and pH3.83 in which the shift of the diffraction lines associated with the variation of pH can be seen, showing how the peak-overlap problem is reduced by the use of a series of different samples.

The use of multiple diffraction patterns having slightly different unit-cell parameters in order to increase the data available for structure refinement needs to be justified. Usually, a change in unit-cell parameters implies a corresponding change in the crystal structure which will be averaged out in this combined fit. Some differences between diffraction patterns have been modelled by allowing the solvent-scattering coefficients to differ for each of the four histograms following the observation that the largest observed differences in peak intensities were mainly at low angles. The remaining differences between model and data were then analysed in terms of the integrated peak intensities computed from the Rietveld refinement. We have computed the correlation coefficient of $\Delta I = (I_{obs} - I_{calc})$ for the four diffraction patterns (Table 2). If the model describes an average of these different data sets then there would be a strong negative correlation of the intensity differences. However, if the differences between model and data are larger than the differences amongst the various data sets then the correlations will be positive. Fig. 12 shows plots of these differences for pairs of data 3 − 4 and 1 − 4. We observe that the correlation coefficient follows the difference in pH and unit-cell parameters between the diffraction patterns, with the smallest value of 0.33 corresponding to the pair of patterns having the largest difference in pH. This positive correlation of 0.33 in the worst case indicates that the differences between the diffraction patterns are smaller than the residual differences remaining after structure refinement.

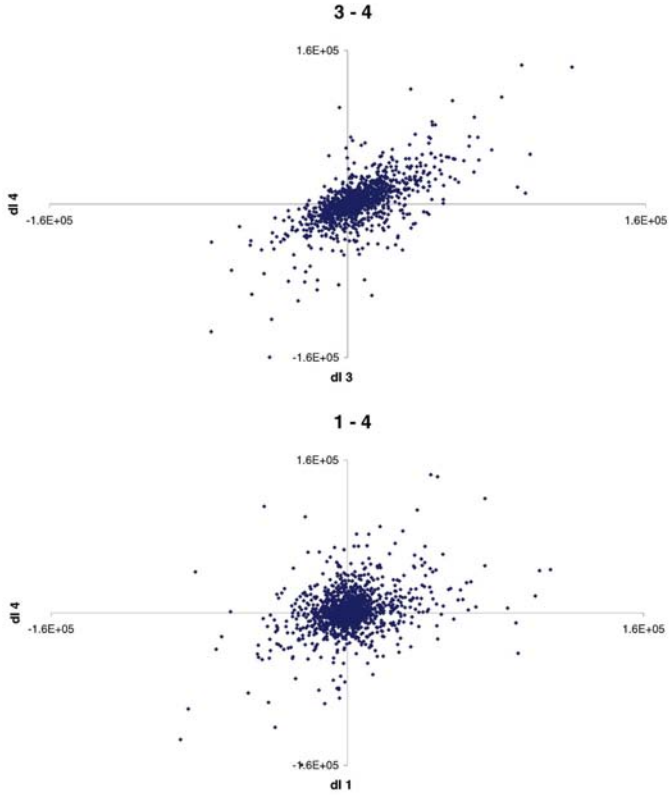

Figure 12
Scatter plots of the regression of the difference between the observed and calculated intensities for some of the profiles involved in the multi-data-set Rietveld refinement (see text).

3.6. Structure description and comparison

In the present study, an average structural model is presented for the description of tetragonal HEWL crystallized in the pH range between 6.56 and 3.33. The starting model for refinement was taken from the refined coordinates (PDB code 193l) of HEWL corresponding to the tetragonal form crystallized at pH 4.3, employing data collected at 279 K (d = 1.33 Å; Vaney *et al.*, 1996). The secondary structure of HEWL (as refined here and assigned using *PyMOL*, DeLano Scientific LLC) is relatively compact and is comprised of seven helices (residues 9–14, 25–35, 80–84, 88–101, 105–107, 109–113 and 120–123) and three β-sheets (residues 44–46, 49–53 and 57–59). The refined molecular conformation and crystal packing are in good agreement with previous structures (Vaney *et al.*, 1996; Von Dreele, 2001). Fig. 13 shows a ribbon diagram depicting the backbone arrangement of the refined structure generated in *PyMOL*. The Ramachandran plot for the main-chain torsion angles (φ, ψ) (Ramakrishnan & Ramachandran, 1965), shown in Fig. 14, indicates that none of the torsion angles fall into disallowed regions. The mean positional error of the refined coordinates was estimated from a Luzzati plot of R factor against 1/d (Luzzati, 1952) to be 0.278 Å using the *SFCHECK* (Vaguine *et al.*, 1999) software and integrated intensities from the Rietveld refinement.

The overall topology and secondary structure of the refined model from powder data is essentially the same as the previously determined single-crystal structure (193l) and two further structures (1ja2 and 1ja6) refined previously from powder data (Von Dreele, 2001; see Table 3 for r.m.s. deviations). One notable difference occurs in the first helix, which is slightly shorter than the equivalent helix in the single-crystal structure. The average r.m.s. deviation of the C^{α}-atom positions after aligning the initial (193l) and refined structures in *Swiss-PdbViewer* is 1.05 Å over 129 residues. Fig. 15 illustrates the r.m.s. deviations between the two models for the main-chain and side-chain atoms of each individual residue. Owing to the different resolution of the experimental data (d = 1.33 Å for 193l and d = 3.27 Å for this refined powder model), together with the different crystallization routes followed, slight differences between the single-crystal and powder structures are to be expected. As Fig. 15 indicates, the largest differences are observed in the N- and C-terminal regions. As described in previous reports, the terminal residues Lys1 and Leu129 exhibit multiple or disordered side-chain conformations (Vaney *et al.*, 1996). Other regions of noticable deviations correspond to the side chain of residue Arg21, a small section of the second helix (residues 25–26) and a flexible loop (residues 74–77) between β3 and helix-3. The side chains of Arg21, as well as those of Arg74 and Arg77, have been reported to be disordered in previous structures.

In order to optimize the refined protein stereochemistry, difference ($2|F_o| - |F_c|$) electron-density maps were generated and used as guides at various stages of the Rietveld refinement (§3.5). The maps were constructed using structure factors extracted from the respective powder diffraction profiles involved in the least-squares minimization procedure. Fig. 16 shows sections of the $2|F_o| - |F_c|$ electron-density map obtained by employing the extracted structure factors from powder data collected for sample pH6.23 (d = 3.312 Å) and the refined structural model. Specific attention was paid to regions of the structure where disorder has been reported previously (Vaney *et al.*, 1996). These regions correspond to flexible loops between residues 61–63, 72–74, 101–103, 124–126 and 128–129 and a small section of helix-4 residues (96–98). As a test of internal consistency for the method, atomic fractions of selected regions of the structure were set to be equal to zero in the Rietveld refinement, modified structure factors were extracted and the maps were regenerated. The use of omit maps reduces the model bias in the maps, verifying that protein powder data contain sufficient information for a medium- to low-resolution structure determination. A comparison of the $2|F_o| - |F_c|$ maps generated when the loop between residues 61–63 was omitted from the model before starting the refinement procedure is shown in Fig. 16(*a*) and indicates that interpretable density returns for this region during the refinement. When omitting regions of the structural model large increases in the profile R factor are observed in the refinement, giving a clear indication that the data are sensitive to fine conformational details in the initial model.

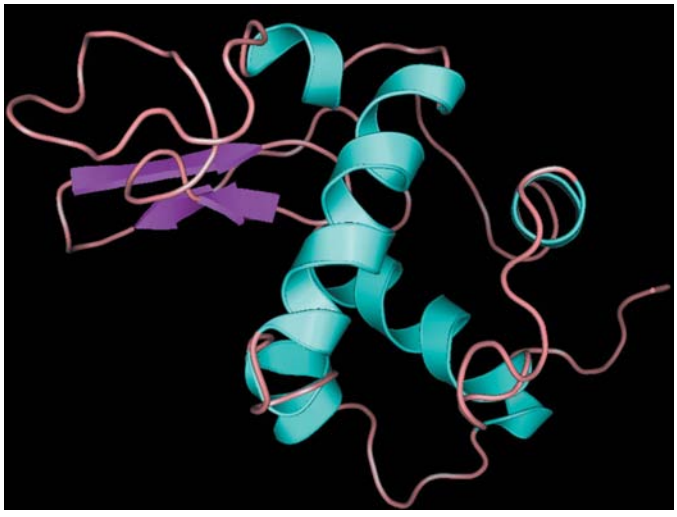

Figure 13
Refined conformation of tetragonal HEWL at 295 K. A total of seven helices and three strands were observed. Individual colours indicate different secondary-structure elements, with cyan, magenta and brown corresponding to helices, β-sheets and coils, respectively.

4. Discussion

In the present report, we focus on the effect of pH on the tetragonal crystal form of HEWL. We have made accurate measurements of the evolution of the unit-cell parameters with pH, which are illustrated by the smooth anisotropic shifts in the peak positions in Fig. 3(*a*). The reproducibility of these

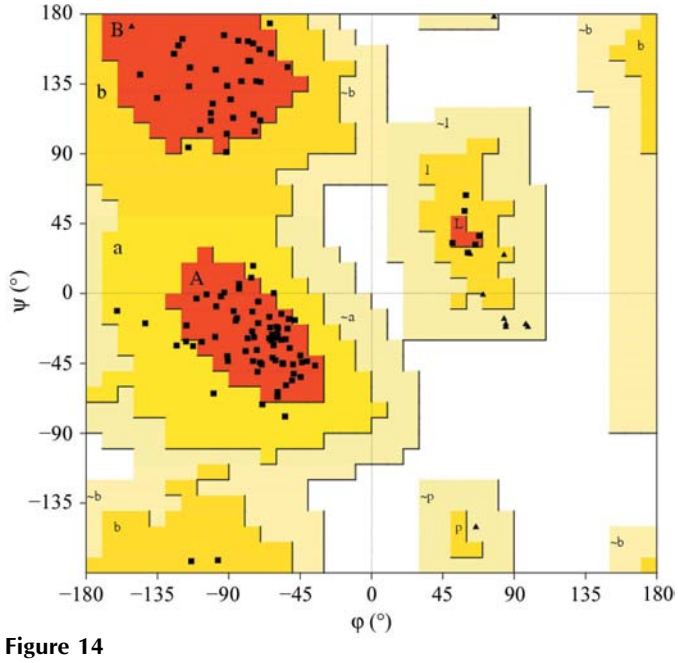

Figure 14
Ramachandran plot for main-chain torsion angles (φ, ψ). Glycine residues are represented by triangles. The shading indicates allowed regions of conformational space: the darker the shading, the more favourable the region. The shaded areas are labelled with respect to the secondary-structural element associated with the region and how favourable the region is: A, a or ~a represents the α-helical region with A being the most favourable; similarly, B, b or ~b represent β-sheet region and 1 or ~1 represent loops.

results and the precision of the powder diffraction data have been verified by carrying out crystallization experiments at both 277 K and RT, where similar behaviour is observed. As a result of the systematic changes in the unit-cell parameters, we believe that the observed variation is an intrinsic property of HEWL and not an artefact as suggested in previous studies (Judge *et al.*, 1999). Changes in unit-cell parameters observed in tetragonal HEWL by varying the temperature for data collection during single-crystal diffraction experiments have been attributed to both slight conformational changes and solvent rearrangements (Kurinov & Harrison, 1995). Similar volume modifications to those reported here have been observed for orthorhombic HEWL by varying the humidity and, as a consequence, the solvent content in the unit cell (Sukumar *et al.*, 1999) or in different enzymes such as rhizopuspepsin, where both conformational and water structure changes were observed with varying pH (Prasad & Suguna, 2003).

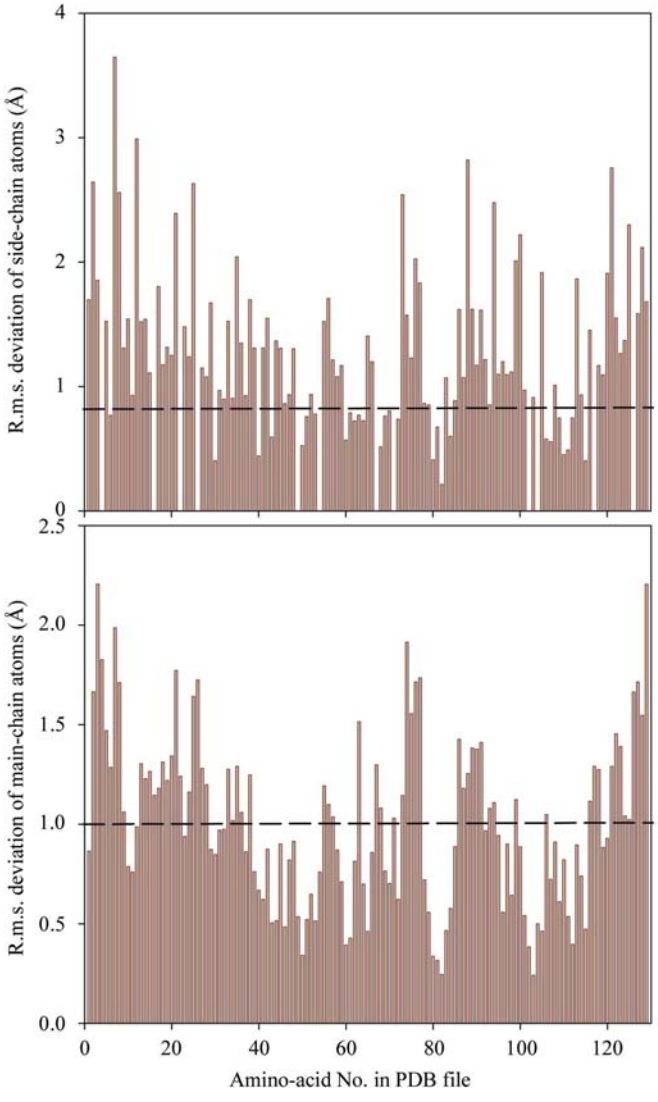

Figure 15
R.m.s. deviations of the main-chain atoms (bottom) and side-chain atoms (top) between the refined and the original 193l models are plotted against residue number. The dashed lines indicate average values.

The molecular structure has been obtained from a multi-pattern Rietveld refinement which exploits the anisotropic variations in unit-cell parameters to reduce the effects of the peak-overlap problem. Our estimates of the data quality and completeness indicate that this methodology gives significant improvements compared with the use of a single diffraction pattern and we have also observed the combined refinement to proceed more smoothly in comparison to a single pattern fit. Analysis of the intensity residuals after refinement showed that the differences between the four patterns (corresponding to different samples) are smaller than the difference between the model and any of the samples, which validates the use of the combined refinement. Variations of the peak intensities as a function of pH were accounted for only by variations in the bulk-solvent parameters, which are difficult to interpret at an atomic level. Our refined structure is similar in topology and stereochemistry to previously determined structures obtained from both single-crystal and powder diffraction data. The largest deviations from previous structures occur in the flexible loop and the N-/C-terminal regions. Additional slight differences between the present structure and other conformations can be attributed to the fact that in this case an average model has been derived for the description of tetragonal HEWL throughout the pH region under study. With the limited resolution of the data, the maps obtained using structure factors extracted from powder data did not clearly reveal any details such as the positions of water molecules in the unit cell or disordered side chains.

The variation of the unit-cell volume with pH is smaller than the anisotropic distortion, indicating that the changes are more likely to arise from a rearrangement of the unit-cell contents rather than the introduction of another chemical species. In the crystal structure the molecules are held together by intermolecular contacts, with solvent channels filling the spaces between them. The largest solvent channels in tetragonal HEWL are oriented parallel to the crystallographic *c* axis. There are three side chains that are involved in forming intermolecular contacts (Moult *et al.*, 1976), Leu129, Asp48 and His15, which have pK values in the pH range covered in this study (Kuramitsu & Hamaguchi, 1980). Kuramitsu and coworkers determined the pK values for these side chains at an ionic strength (precipitant) of 0.1 *M* at 298 K to be 3.1, 4.3 and 5.8 for Leu129, Asp48 and His15, respectively. They reported that the pK values increased slightly with ionic strength and the pK trends have since been extrapolated in studies which explored similar conditions to those used here (Judge *et al.*, 1999) to provide an estimate of the increase in pK for these side chains in the region of ∼0.1–0.3 pH units. It seems plausible that localized changes in molecular-charge distribution caused by the titration of charged groups on these side chains may modify the strength of the intermolecular interactions and could be manifested in the change in unit-cell parameters we observed over the pH range 3–6.5. It is beyond the scope of the present study to refine the structures resulting from the different pH conditions individually; however, minor localized changes in the lattice contacts involving these residues may arise in structures at pH 3 and 6.5. Several previous

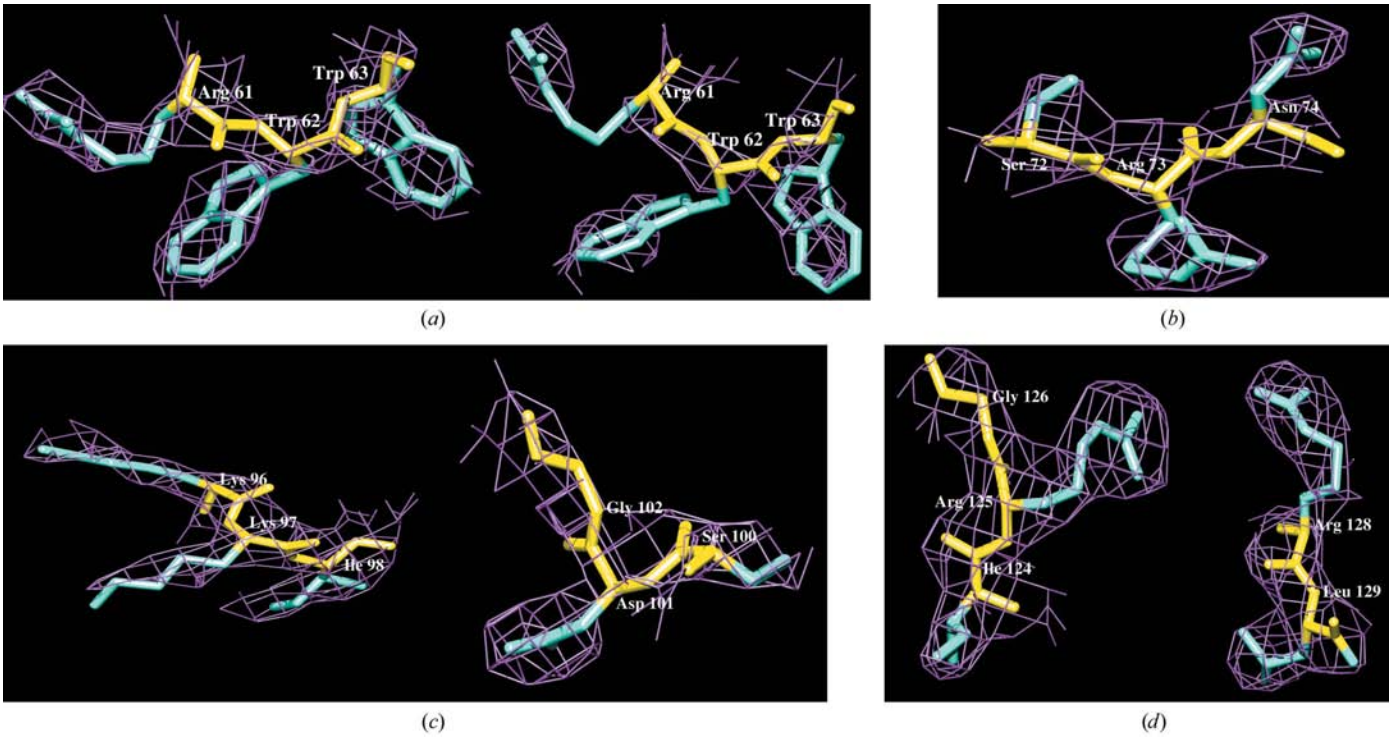

Figure 16
Perspective views of selected regions of the final $2|F_o| - |F_c|$ electron-density maps for tetragonal HEWL at 3.27 Å resolution with the contour level at 1σ. (*a*) Loop 61–63 when this part of the structure was not omitted (left) and was omitted from the refinement procedure (right), (*b*) loop 72–74, (*c*) helix 96–98 (left) and loop 101–103 (right) and (*d*) loops 124–126 (left) and 128–129 (right). The selected regions correspond to those characterized by disorder according to earlier reports. These figures were prepared with the *CCP*4 molecular-graphics program v.0.6.

reports have suggested that net changes in surface-charge distribution induced by fine increments in pH influence nucleation rates (McPherson, 1982) as well as crystal size and axial ratios (Judge *et al.*, 1999).

The presence of the orthorhombic form at 277 K suggests that the phase transition occurs at least 1.0–1.5 pH units above the transition observed at RT when all other parameters are held constant. However, Berthou & Jollès (1974) have shown the persistence of the nucleation and growth of orthorhombic crystals in solutions that were cooled to 277 K after having been warmed to temperatures at or above the base transition temperature (*i.e.* 298 K). Since the diffraction data presented here were collected at room temperature, it is possible that the orthorhombic phase precipitated after warming the samples. The observation that the orthorhombic form was observed in this study only at the highest pH levels examined (samples pH6.56, pH6.51 and pH6.41) may relate to the decreased solubility of the orthorhombic form at higher pH levels reported by Ewing *et al.* (1994). Previous studies have demonstrated that the width of the metastable zone varies with pH for both forms of HEWL (Ewing *et al.*, 1994; Carpineti & Piazza, 2004).

We believe that this kind of systematic approach further extends the viability of powder diffraction methods for research on macromolecular systems. The use of robotic automation for data collection was an important factor in designing this study and the recently installed capillary-changing robot at the ID31 beamline (which can take up to 50 samples at a time) is an excellent precursor for further progress. In the present study 24 samples were measured *via* an automated procedure in less than 7 h, providing extremely high-quality powder data. The low instrumental contribution to the diffraction lines and the high precision of the determination of unit-cell parameters allowed small variations of the unit-cell parameters with varying pH to be quantified precisely. The use of a systematic variation of sample-preparation conditions is likely to be particularly useful for the detection of protein–ligand complex formation by variations of ligand concentration (Von Dreele, 2001, 2005). The optimization of cryoprotection conditions and preparation of heavy-atom derivatives could also exploit systematic powder experiments.

In conclusion, we have observed systematic variations in the tetragonal unit cell of HEWL as a function of the pH used for crystallization at both 277 K and RT. This result might be indicative of solvent rearrangements, slight changes of the protein conformation or changes in packing contacts. While the powder data give clear results pertaining to the unit-cell parameters, the electron density is not of high enough quality to distinguish between these possibilities. We were able to account for the data at all pH values without any conformational rearrangements, although this possibility cannot be ruled out. At the current level of analysis, our observations are consistent with the changes in unit-cell parameters being the result of a reorganization of the water structure, which is anticipated to have an effect on the unit-cell parameters of the

same order of magnitude and would be consistent with the observed changes in bulk-solvent parameter; however, minor modifications in specific packing contacts may also be a contributing factor and may well be linked to reorganization of the water structure by changing the dimensions of specific solvent channels.

We would like to thank ESRF for provision of beam time on the ID31 beamline. We are grateful to R. B. Von Dreele for the *GSAS* software used for structure refinements and many invaluable discussions.

References

Berthou, J. & Jollès, P. (1974). *Biochim. Biophys. Acta*, **336**, 222–227.
Biswal, B. K., Sukumar, N. & Vijayan, M. (2000). *Acta Cryst.* D**56**, 1110–1119.
Boultif, A. & Louër, D. (1991). *J. Appl. Cryst.* **24**, 987–993.
Brunelli, M., Wright, J. P., Vaughan, G. B. M., Mora, A. J. & Fitch, A. N. (2003). *Angew. Chem. Int. Ed.* **42**, 2029–2032.
Carpineti, M. & Piazza, R. (2004). *Phys. Chem. Chem. Phys.* **6**, 1506–1511.
Collaborative Computational Project, Number 4 (1994). *Acta Cryst.* D**50**, 760–763.
David, W. I. F., Shankland, K. & Shankland, N. (1998). *J. Chem. Soc. Chem. Commun.*, pp. 931–932.
Ewing, F., Forsythe, E. & Pusey, M. (1994). *Acta Cryst.* D**50**, 424–428.
Finger, L. W., Cox, D. E. & Jephcoat, A. P. (1994). *J. Appl. Cryst.* **27**, 892–900.
Fitch, A. N. (2004). *J. Res. Natl Inst. Stand. Technol.* **109**, 133–142.
Guex, N. & Peitsch, M. C. (1999). *Swiss-PdbViewer*. Glaxo Wellcome Experimental Research. http://www.expasy.ch/spdbv.
Hooft, R. W. W., Vriend, G., Sander, C. & Abola, E. E. (1996). *Nature (London)*, **381**, 272.
Jollès, P. & Berthou, J. (1972). *FEBS Lett.* **23**, 21–23.
Judge, R. A., Jacobs, R. S., Frazier, T., Snell, E. H. & Pusey, M. L. (1999). *Biophys. J.* **77**, 1585–1593.
Kuramitsu, S. & Hamaguchi, K. (1980). *J. Biochem.* **87**, 1215–1219.
Kurinov, I. V. & Harrison, R. W. (1995). *Acta Cryst.* D**51**, 98–109.
Larson, A. C. & Von Dreele, R. B. (2004). *General Structure Analysis System (GSAS)*. Los Alamos National Laboratory Report LAUR 86-748.
Laskowski, R. A., MacArthur, M. W., Moss, D. S. & Thornton, J. M. (1993). *J. Appl. Cryst.* **26**, 283–291.
LeBail, A., Duroy, H. & Fourquet, J. L. (1988). *Mater. Res. Bull.* **23**, 447–452.
Luzzati, V. (1952). *Acta Cryst.* **5**, 802–810.
McPherson, A. (1982). *Preparation and Analysis of Protein Crystals*, pp. 98–99. New York: John Wiley.
Margiolaki, I., Wright, J. P., Fitch, A. N., Fox, G. C. & Von Dreele, R. B. (2005). *Acta Cryst.* D**61**, 423–432.
Markvardsen, A. J., David, W. I. F., Johnson, J. C. & Shankland, K. (2001). *Acta Cryst.* A**57**, 47–54.
Moult, J., Yonath, A., Traub, W., Smilansky, A., Podjarny, A., Rabinovich, D. & Saya, A. (1976). *J. Mol. Biol.* **100**, 179–195.
Pawley, G. S. (1981). *J. Appl. Cryst.* **14**, 357–361.
Potterton, E., Briggs, P., Turkenburg, M. & Dodson, E. (2003). *Acta Cryst.* D**59**, 1131–1137.
Prasad, B. V. L. S. & Suguna, K. (2003). *Acta Cryst.* D**59**, 1755–1761.
Ramakrishnan, C. & Ramachandran, G. N. (1965). *Biophys. J.* **5**, 909–933.
Rietveld, H. M. (1969). *J. Appl. Cryst.* **2**, 65–71.
Rodriguez-Carvajal, J. (1993). *Physica B*, **192**, 55–69.
Sivia, D. S. (2000). *J. Appl. Cryst.* **33**, 1295–1301.
Sauter, C., Otálora, F., Gavira, J.-A., Vidal, O., Giegé, R. & García-Ruiz, J. M. (2001). *Acta Cryst.* D**57**, 1119–1126.
Shankland, K., David, W. I. F. & Sivia, D. S. (1997). *J. Mater. Chem.* **7**, 569–572.
Sukumar, N., Biswal, B. K. & Vijayan, M. (1999). *Acta Cryst.* D**55**, 934–937.
Toby, B. H. (2001). *J. Appl. Cryst.* **34**, 210–213.
Vagin, A. A. & Teplyakov, A. (1997). *J. Appl. Cryst.* **30**, 1022–1025.
Vaguine, A. A., Richelle, J. & Wodak, S. J. (1999). *Acta Cryst.* D**55**, 191–205.
Vaney, M. C., Maignan, S., Riès-Kautt, M. & Ducruix, A. (1996). *Acta Cryst.* D**52**, 505–517.
Von Dreele, R. B. (1999). *J. Appl. Cryst.* **32**, 1084–1089.
Von Dreele, R. B. (2001). *Acta Cryst.* D**57**, 1836–1842.
Von Dreele, R. B. (2005). *Acta Cryst.* D**61**, 22–32.
Von Dreele, R. B., Stephens, P. W., Smith, G. D. & Blessing, R. H. (2000). *Acta Cryst.* D**56**, 1549–1553.
Wright, J. P. (2004). *Z. Kristallogr.* **219**, 791–802.
Wright, J. P. (2005). In preparation.
Wright, J. P. & Forsyth, J. B. F. (2000). Rutherford Appleton Laboratories Report RAL-TR-2000–012.